Hindawi
Advances in Civil Engineering
Volume 2020, Article ID 2898971, 11 pages
https://doi.org/10.1155/2020/2898971

Research Article

Study on Law of Overlying Strata Breakage and Migration in Downward Mining of Extremely Close Coal Seams by Physical Similarity Simulation

Xiaobin Li, Wenrui He, and Zhuhe Xu

School of Energy and Mining Engineering, China University of Mining and Technology (Beijing), Beijing 100083, China

Correspondence should be addressed to Xiaobin Li; lxb162197@126.com

Received 3 September 2019; Revised 9 November 2019; Accepted 7 January 2020; Published 14 February 2020

Academic Editor: Fan Gu

Extremely close coal seam groups are widely distributed in China, and the main mining method is downward mining. In the downward mining process of extremely close coal seam groups, the violent movement of overlying strata will cause the redistribution of surrounding rock stress. It not only produces stress concentration on the pillar but also causes the roof of the lower coal seam to be broken and difficulty in maintaining the mining roadway. In this study, the physical similitude modeling method and field observations were used to study the breakage and migration law of overlying strata in the downward mining of extremely close coal seams. Results show that in the process of mining upper coal seam, the first weighting step of the main roof is 37.5 m and the periodic weighting step is 12.5 m. The occurrence of strata separation is beneficial to the prediction of roof weighting. When the working face advances to 25 m, the rock stratum approximating a parallelogram of height 5 m does not collapse, and the working face is relatively dangerous. When mining the lower coal seam, the overall pressure of the working face is large, but the periodic weighting of the working face is not obvious. The first collapse step of the immediate roof is 15 m. When mining the upper and lower coal seams, the subsidence of the monitoring point increases significantly at 17.5 and 15 m, respectively. The roof collapse of the lower coal seam occurs 2.5 m ahead of that of the upper coal seam. The hydraulic value of the support, roof fall height, and sloughing depth in the entire working face reach the maximum at the coal pillar, and the extreme points at the coal pillar are relatively concentrated. This research provides some guidance for the safe and efficient mining of extremely close coal seams in the future.

1. Introduction

China produces and consumes the most amount of coal in the world [1]. The proportion of coal in primary energy production and consumption is approximately 70%. According to the British Petroleum Statistical Review of World Energy 2018 program, China's coal output reached 3.523 billion tons in 2017, accounting for 45.6% of the world's total output [2]. Therefore, coal is important for China's economic development [3]. Recently, with large-scale mining, coal seams with good geological conditions have been gradually exhausted [4]. Owing to the large proportion of extremely close coal seams in China, the mining of extremely close coal seams is becoming more common for improving the utilization of coal resources [5]. Extremely close coal seams are closely spaced and interact with each other during mining. With the decrease in spacing, the interaction between coal seams will gradually increase [6]. When the distance of coal seams is extremely close, the roof integrity of the lower coal seam will be damaged by the mining of the upper coal seam. The area above the roof is the caving zone formed by the collapsed immediate roof [7]. Moreover, the remaining pillars in the upper coal seam can easily cause stress concentration [8, 9]. Consequently, the roof structure and stress environment in the mining area of the lower coal seam changed, and many new mine pressure phenomena occurred during the mining of extremely close coal seams [10].

Many engineering examples show that the violent movement of overlying strata will induce serious air leakages

and water and gas accidents [11, 12]. Factors such as mining thickness, burial depth, and dip angle of coal seam are closely related to the law of overlying strata movement [13]. Because the process of strata movement is complex and no theoretical analysis method exists to satisfy engineering practices [14], physical similarity simulation is still the main method to study strata movement. This method overcomes the invisibility of mine pressure and overlying strata movement in field production, reflects the mechanical phenomenon visually, and can simulate the entire process in a short time. Based on physical similarity simulations, Huang et al. [15] studied the characteristics of overlying strata movement and strata behavior law in fully mechanized coal mining and backfilling longwall faces. Yuan et al. [16] proposed a new method for a similar material simulation experiment of steeply inclined upper protective layer mining and successfully applied it to the Nantong mining district. Niu et al. [17] constructed a similar physical model of coal rock to verify that a new method could be applied for the monitoring and early warning of coal and rock dynamic disasters. Zhang et al. [18] discussed the roof movement law of a fully mechanized mining face under a large dip angle through physical similarity simulations. Based on the engineering background of the Wuhushan coal mine, the law of overlying strata breakage and migration in the downward mining of extremely close coal seams was studied using the physical similitude modeling method. The current study can provide important guidance for the safe and efficient mining of extremely close coal seams in the future.

Recently, experts and scholars have performed relevant research and exploration on the mining system and safety technology of extremely close coal seams. Based on a mechanical model and FLAC 3D numerical simulations, Wu et al. [19] studied the stress distribution under a coal pillar and optimized the roadway layout. Based on the in situ monitoring of overburden failure, Ning et al. [20] proposed a statistical formula for predicting the maximum height of overburden failure induced by extremely close coal seam mining. Zhang et al. [21] discussed the relationship between pillar size and roadway stability, incorporating a strain softening model for pillars and a double yield model for goaf material. By considering horizontal, vertical, and tangential stresses, Yan et al. [22] and Yuan et al. [23] proposed a new method for calculating the stress distribution of coal pillars. Based on experimental research and the UDEC software, Zhang et al. [24] analyzed the relationship between mining sequence under water body and overburden failure degree. Zhang et al. [25] incorporated geotechnical considerations for concurrent pillar recovery in extremely close coal seams, where mining sequence, panel layout, and pillar size were considered. Based on the observations of surface subsidence and three-dimensional simulations, Yu et al. [26] and Zhu et al. [27] studied the relationship between upper coal pillar and lower working face. Based on the floor failure mechanics model, Zhang et al. [28] proposed a new method to monitor floor failure depth and successfully applied it to the Caocun coal mine in China. Liu et al. [29] deduced a formula for the analysis of floor stress distribution and roadway position in extremely close coal seams. Aiming at the large deformation and destruction of roadway in extremely close coal seams, Li et al. [30] proposed an asymmetric support scheme, which has been successfully applied in other mines. Based on the finite element method, Ghabraie et al. [31] and Khanal et al. [32] developed a new method that can accurately simulate the collapse of overlying strata and surface subsidence during multiseam mining. Based on the law of gas occurrence and outburst characteristics, Wang et al. [33] and Konicek and Schreiber [34] studied the sequence of coal seam mining, key protective seam mining technology, and gas control measures.

As described above, scholars primarily focused on the layout of mining roadways in the lower coal seam, gas control, mining sequence, and stress distribution of pillars and floor in the upper coal seam. However, studies regarding the breakage and migration law of overlying strata by physical similarity simulations are rare. Therefore, the law of strata breakage and migration must be studied to realize the safe and efficient mining of extremely close coal seams.

2. Engineering Background

2.1. Mining and Geological Condition. The Wuhushan coal mine, located in Wuhai city, Inner Mongolia autonomous region, China (Figure 1), covers a mining area of 12.6 km^2. Coals 9 and 10 are extremely close coal seams, with a 0.45–5.02 m layer of sandy mudstone in the middle. The inclination and strike length of the working face are 130 and 400 m, respectively. A fully mechanized mining method was adopted. The average thickness of coal 9 was 3.2 m. The rock strata above coal 9 were mudstone of average thickness 9.4 m and medium sandstone of average thickness 6.0 m, while the rock stratum below coal 9 was sandy mudstone of average thickness 2.0 m. The average thickness of coal 10 was 2.2 m. Its roof was also the floor of coal 9, and the rock stratum below coal 10 was siltstone of average thickness 5.4 m. Figure 2 shows the generalized stratigraphy column.

2.2. Experiments for Determining Rock Mechanical Properties. To understand the rock mechanical properties better, the coal and rock mass in the field were processed into a certain shape using the ZS-100 fully automatic drilling machine, SCM200 double-end grinder, HJD-150A concrete sawing machine, and SC200 automatic core-taking machine. Figure 3 shows the coal and rock samples for use in experiments. Figure 4 shows the processing equipment. Uniaxial compression, splitting, and shear strength tests were performed on the samples to determine the mechanical parameters of coal and rock mass [35], as shown in Table 1.

3. Similar Material Simulation

3.1. Similarity Theory. A similar material simulation was performed based on the similarity theory. Geometric, time, and dynamic similarities must be considered between the model and prototype. Based on [18] and "dimensional analysis," the dynamic similarity rate is presented as shown in equation (4). Meanwhile, Ren et al. [36] indicated that the dynamic similarity requires the force of the model and

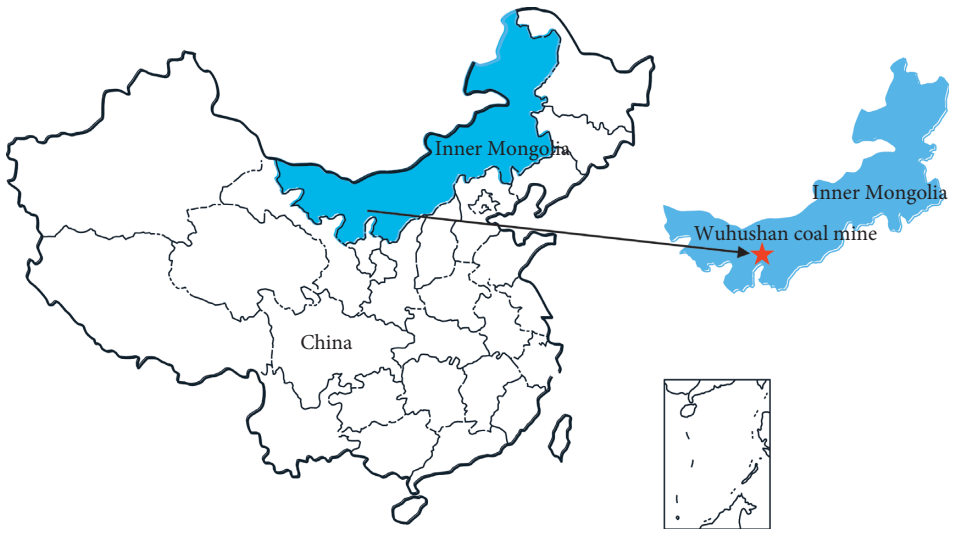

Figure 1: Location of Wuhushan coal mine in Inner Mongolia autonomous region, China.

Stratigraphic column	Lithology	Thickness (m)	Lithological description
	Medium sandstone	(3.23~7.61)/ 6.0	It is mainly siltstone and fine sandstone.
	Mudstone	(5.14~13.19)/ 9.4	It is generally gray with yellow-brown calcareous sandstone and iron nodules.
	Coal 9	(1.19~4.61)/ 3.2	The structure is simple, and the fissures are well developed. It belongs to a relatively stable coal seam.
	Sandy mudstone	(0.45~5.02)/ 2.0	The main features are grey-black mudstone, loose cementation, poor separation and grinding roundness, local gravel, and high mica content.
	Coal 10	(2.03~2.56)/ 2.2	The structure is simple, and the fissures are well developed, with an average thickness of 2.2 m.
	Siltstone	(2.39~6.63)/ 5.4	It is mainly siltstone and fine sandstone, with a thin layer of coal at the top.

Figure 2: Generalized stratigraphy column of the test site.

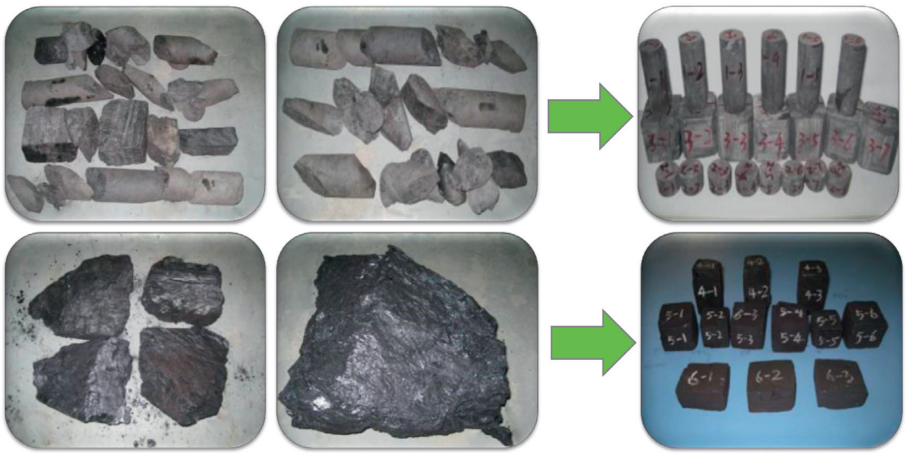

Figure 3: Coal and rock samples used in the experiments.

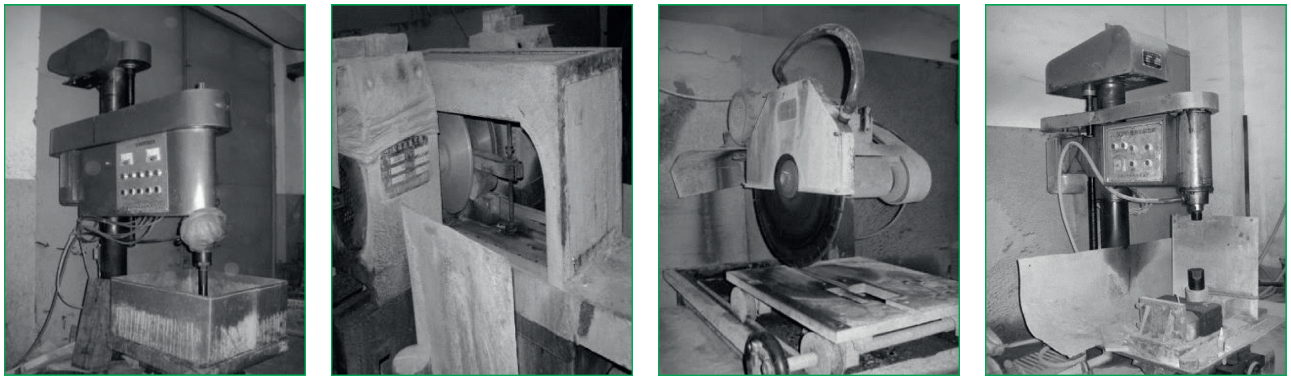

(a) (b) (c) (d)

Figure 4: Processing equipment: (a) ZS-100 fully automatic drilling machine; (b) SCM200 double-end grinder; (c) HJD-150A concrete sawing machine; (d) SC200 automatic core-taking machine.

Table 1: Mechanical properties of coal-rock strata.

Number	Lithology	Density (kg/m^3)	Shear modulus (GPa)	Bulk modulus (GPa)	Cohesion (MPa)	Friction angle (°)	Tensile strength (MPa)
1	Fine sandstone	2540	5.08	6.25	10.1	27	6.6
2	Siltstone	2640	5.82	6.09	7.9	28	7.1
3	Fine sandstone	2540	5.08	6.25	10.1	27	6.6
4	Sandy mudstone	2200	3.6	6.0	3.0	32	5.9
5	Siltstone	2640	5.82	6.09	7.9	28	7.1
6	Mudstone	2220	1.3	3.0	0.8	32	5.9
7	Medium sandstone	2540	5.91	6.81	10.7	31	6.5
8	Mudstone	2220	1.3	3.0	0.8	32	5.9
9	Coal 9	1400	0.76	1.6	2.65	25	1.8
10	Sandy mudstone	2200	3.6	6.0	3.0	32	5.9
11	Coal 10	1400	0.76	1.6	2.65	25	1.8
12	Siltstone	2640	5.82	6.09	7.9	28	7.1

prototype at the corresponding point and time to be at a certain proportion to each other, and the main characteristics of force are reflected by compressive strength and bulk density in the experiment. Therefore, the compressive strength can be described as the dynamic similarity rate.

The geometric similarity rate of the model is

$$C_L = \frac{L_m}{L_p} = \frac{1}{50}, \tag{1}$$

where C_L refers to the length similarity constant and L_m and L_p are the lengths of the similar material simulation model and prototype, respectively.

The time similarity rate of the model is

$$C_T = \frac{T_m}{T_p} = \sqrt{C_L} = \frac{1}{7}, \tag{2}$$

where C_T is the time similarity constant and T_m and T_p are the time of the similar material simulation model and prototype, respectively.

The density similarity rate of the model is

$$C_\rho = \frac{\rho_m}{\rho_p} = \frac{1}{1.6}, \tag{3}$$

where $C\rho$ is the density similarity constant and ρ_m and ρ_p are the densities of the similar material simulation model and prototype, respectively.

The dynamic similarity rate of the model is

$$C_\sigma = \frac{F_m}{F_p} = \frac{m_m\left(dv_m/dt_m\right)}{m_d\left(dv_d/dt_d\right)} = \frac{\sigma_m}{\sigma_p} = \frac{L_m}{L_p}\frac{\gamma_m}{\gamma_p} = \frac{L_m}{L_p}\frac{\rho_m}{\rho_p} = \frac{1}{80}, \tag{4}$$

where C_σ is the strength similarity constant and σ_m, σ_p, γ_m, and γ_p are the compressive strengths and bulk densities of the similar material simulation model and prototype, respectively.

According to the dynamic similarity rate formula, the compressive strength and bulk density of the strata in the model and prototype can be obtained (Table 2).

3.2. Overall Design of Physical Similarity Model. Based on the actual geological data of the fully mechanized mining face of the Wuhushan coal mine, fine sand, lime, and gypsum were selected as similar materials. The size of the test bench was 1800 mm (length) × 160 mm (width) × 1300 mm (height), and the plane stress model was adopted. The model building process is presented as follows [37]: (1) based on the calculation in Table 3, sand, lime, and gypsum were weighed

Table 2: Mechanics parameters of the similar rock material.

Number	Lithology	Prototype		Model	
		Bulk density (g/cm^3)	Compressive strength (MPa)	Bulk density (g/cm^3)	Compressive strength (MPa)
1	Fine sandstone	2.54	75.3	1.588	0.941
2	Siltstone	2.64	50.5	1.65	0.631
3	Fine sandstone	2.54	75.3	1.588	0.941
4	Sandy mudstone	2.2	30.2	1.375	0.377
5	Siltstone	2.64	44.2	1.65	0.553
6	Mudstone	2.22	32	1.388	0.400
7	Medium sandstone	2.54	85	1.588	1.063
8	Mudstone	2.22	30.1	1.388	0.377
9	Coal 9	1.4	9.5	0.875	0.119
10	Sandy mudstone	2.2	30.2	1.375	0.377
11	Coal 10	1.4	9.5	0.875	0.119
12	Siltstone	2.64	50.5	1.65	0.631

Table 3: Similar simulation strata distribution and material mixture ratio.

Number	Lithology	Thickness (mm)	Proportioning	Material consumption (kg)			
				Sand	Lime	Gypsum	Water
1	Fine sandstone	136.0	9 : 6 : 4	56.402	3.760	2.507	2.507
2	Siltstone	88.0	8 : 7 : 3	36.045	3.154	1.352	1.622
3	Fine sandstone	30.0	9 : 6 : 4	12.442	0.829	0.553	0.553
4	Sandy mudstone	106.0	10 : 7 : 3	44.404	3.108	1.332	1.954
5	Siltstone	152.0	9 : 8 : 2	63.037	5.603	1.401	2.802
6	Mudstone	84.0	8 : 8 : 2	34.406	3.441	0.860	1.548
7	Medium sandstone	120.0	8 : 6 : 4	49.152	3.686	2.458	2.212
8	Mudstone	188.0	10 : 7 : 3	78.755	5.513	2.363	3.465
9	Coal 9	64.0	10 : 9 : 1	26.810	2.413	0.268	1.180
10	Sandy mudstone	40.0	10 : 7 : 3	16.756	1.173	0.503	0.737
11	Coal 10	44.0	10 : 9 : 1	16.756	1.508	0.168	0.737
12	Siltstone	100.0	7 : 5 : 5	16.128	1.152	1.152	0.737

and combined in a mixer. (2) The mixed material was paved evenly and compacted to maintain the required bulk density. Subsequently, mica powder was sprinkled on the strata to clarify the model bedding. (3) The other strata of the model followed the preceding steps until the required height was reached. (4) The weight of the overlying strata above the model was determined by adding the counterweight. (5) The model was dried naturally for five days.

Because the thickness and strength of the floor of coal 10 will not significantly affect the test, they can be simplified during building. The average height was 200 m from the actual working face to the surface. The thickness of the simulated overlying strata was 45.2 m, and the remaining height of 154.8 m was generated by the simulated pressure. The total height of this test was 1148 mm. The total excavation length was 1000 mm, and the length of each excavation was 50 mm. During building, the actual size of the strata should be adhered strictly. The specific amount of similar material is shown in Table 3.

3.3. Layout of Monitoring Points. To acquire the displacement variation of the overlying strata, displacement monitoring points were evenly arranged. An electronic theodolite with high precision was used to measure strata movement during mining. As shown in Figure 5, the monitoring points were evenly arranged above the roof of coal 10. Six detection lines were arranged in the model, namely, 2, 12, 22, 32, 42, and 52 cm from Coal 9. A total of 11 monitoring points were set on each line. A 15 cm × 10 cm grid design was adopted. To acquire data accurately during mining, a data collector was used to record the pressure data automatically; subsequently, the data are transmitted to a computer for analysis, as shown in Figure 6.

4. Mining Result Analysis of Upper Coal Seam

4.1. Mine Pressure Appearance Law. The open-off cut of the working face is 7.5 m. When the working face advances to 17.5 m, the first collapse of the immediate roof occurs. The collapse height is 2.5 m. As shown in Figure 7, when the working face advances to 25 m, the mining-induced fracture will not extend to the main roof. The collapsed strata form a two-part masonry beam articulated structure. The collapse height is 5 m, which is approximately 1.5 times the mining height. The upper minimum collapse range is 10 m. Because of its self-stabilization ability, the strata approximating a parallelogram did not collapse. However, when the working face advances to 27.5 m, the first collapse of the main roof occurs. The working face encounters the first weighting of the main roof. As shown in Figure 8, the overlying strata

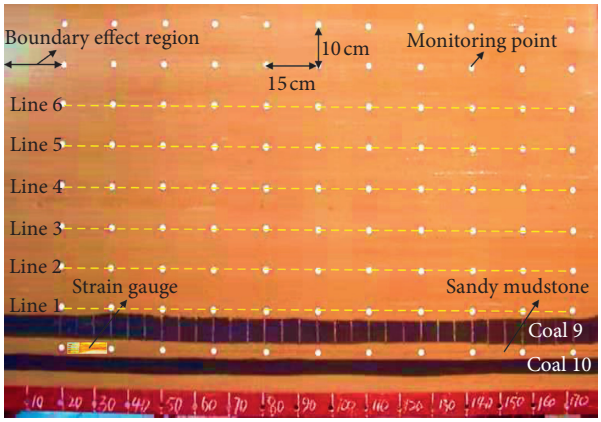

Figure 5: Similar simulation model and layout of monitoring points.

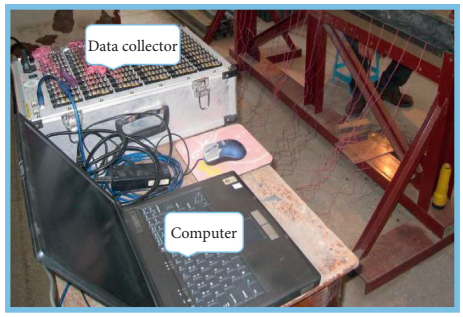

Figure 6: Data acquisition device.

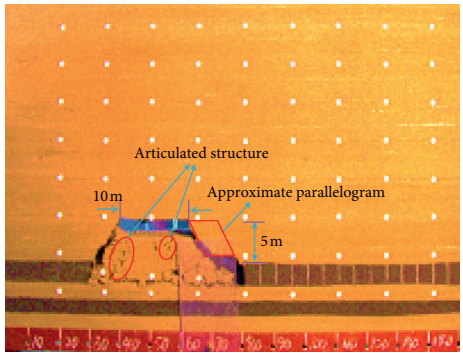

Figure 7: 25 m advancement.

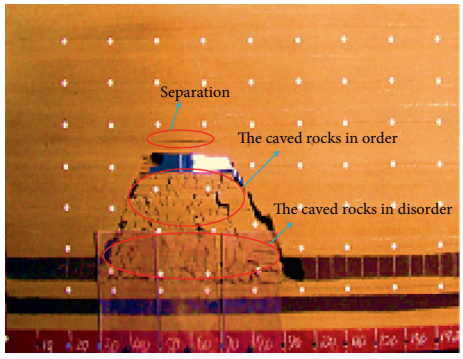

Figure 8: 32.5 m advancement.

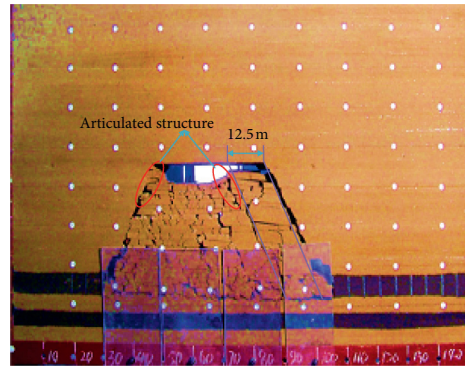

Figure 9: 37.5 m advancement.

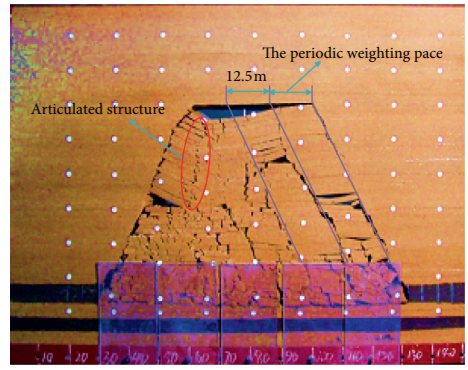

Figure 10: 50 m advancement.

begin to separate when the working face advances to 32.5 m. The first periodic weighting of the main roof occurs when the working face advances to 37.5 m (Figure 9). The second periodic weighting of the main roof occurs when the working face advances to 50 m (Figure 10). The average periodic weighting step is 12.5 m.

From the discussion above, it is clear that with the advance of the working face, the first collapse of the immediate roof and the first and periodic weighting of the main roof will occur. Finally, the overlying strata will collapse in a large area. When the periodic weighting of the main roof occurs, the collapsed roof will exhibit a specific regularity. The collapse length of the overlying strata is the same, which is approximately equal to the periodic weighting step. From the working face up, the collapsed strata become more orderly and a stable articulated structure can be formed easily. This is because the strength of the first collapsed strata is low, and with the advance of the working face, the collapsed strata are gradually crushed by the strata above.

4.2. Analysis of Roof Subsidence. As shown in Figure 11, the subsidence of the overlying strata shows a certain regularity. The maximum and uniform subsidence is line 1, which is 2 cm from coal 9. The variation range is between 55 and 64 mm, which is close to coal seam thickness. The maximum subsidence of lines 2, 3, 4, 5, and 6 is 48, 45, 42, 36, and 26 mm, respectively. This shows that the subsidence of the overlying strata decreases with the increase in distance from

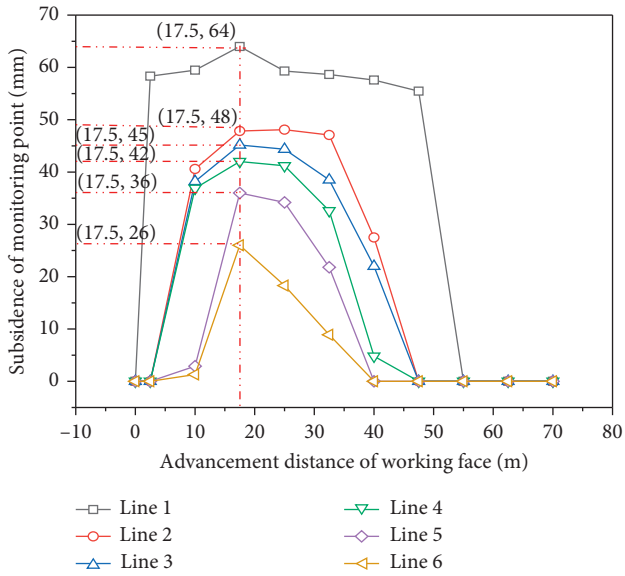

Figure 11: Subsidence of monitoring points.

the coal seam. This is because with the increase in distance from the coal seam, the probability of interaction increases between the collapsed overlying strata. In addition, some stable structures may be formed between the large strata. Consequently, the space between the strata and the dilatancy coefficient increase. Ultimately, the subsidence of the overlying strata is reduced. When the advancement distance of the working face is 17.5 m, the subsidence of the monitoring point increases significantly. This phenomenon is caused by a sudden roof caving in the gob, which is consistent with the physical similarity simulation results.

5. Mining Result Analysis of Lower Coal Seam

5.1. Mine Pressure Appearance Law. When the lower coal seam was mined, the overlying strata and the roof of the upper coal seam collapsed and recemented. Owing to the mining activity of the upper coal seam, the roof of coal 10 was damaged and generated some microfractures; additionally, the roof strength was low. Therefore, the first collapse of the immediate roof occurred at 15 m during mining. The roof collapse of the lower coal seam was 2.5 m ahead of that of the upper coal seam. In the subsequent mining process, no obvious periodic weighting of the main roof occurred, the roof falls with mining, and no obvious structure was formed, as shown in Figure 12.

5.2. Analysis of Roof Subsidence. As shown in Figures 11 and 13, the subsidence of the overlying strata has little effect on the outside of the mining area. However, the subsidence of the overlying strata above the mining area changed significantly. Most of the subsidence was concentrated between 80 and 104 mm. The subsidence of lines 1, 2, and 3 was approximately equal to the thickness of Coal 10. Owing to effect of mining, the original structure of the overlying strata was destroyed and the subsidence of the upward detection lines increased. Ultimately, the collapsed strata's dilatancy

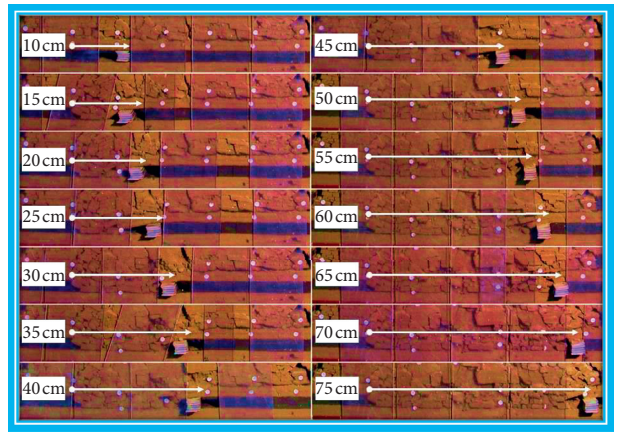

Figure 12: Roof collapse patterns at different distances.

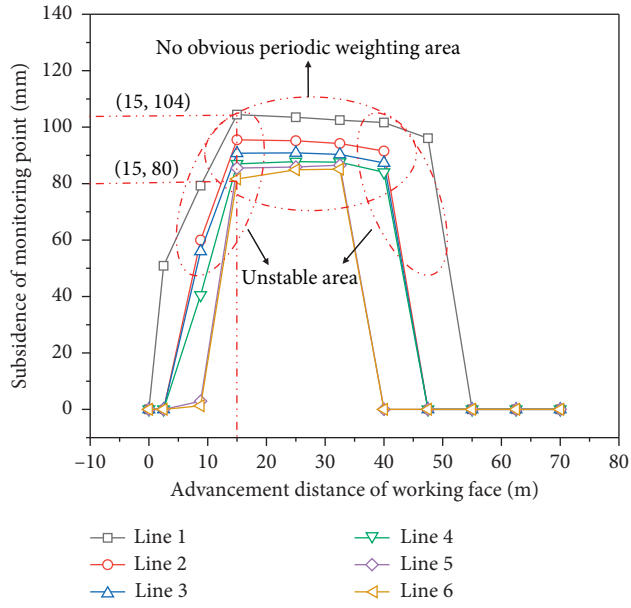

Figure 13: Subsidence of monitoring points.

coefficient would be reduced, and the rock mass further compacted. The increase in the sinking point of lines 4, 5, and 6 exceeded the coal seam thickness after mining Coal 10, and the maximum increase could reach to 227.9%. This was caused by the decrease in the coefficient of fragmentation and expansion. Meanwhile, it could be attributed to Coal 10 being directly excavated before the strata movement had stopped completely. As shown in Figure 13, when the advancement distance of the working face is 15 m, the subsidence of the monitoring point increases sharply and the roof collapses in a large area. The subsidence curve is approximately symmetric, with an unstable area on both sides and no obvious periodic weighting area in the middle.

6. Field Observation

6.1. Layout of Stations. To understand the law of mine pressure in extremely close coal seams, the mine pressure in 1001 working face of the Wuhushan coal mine was observed.

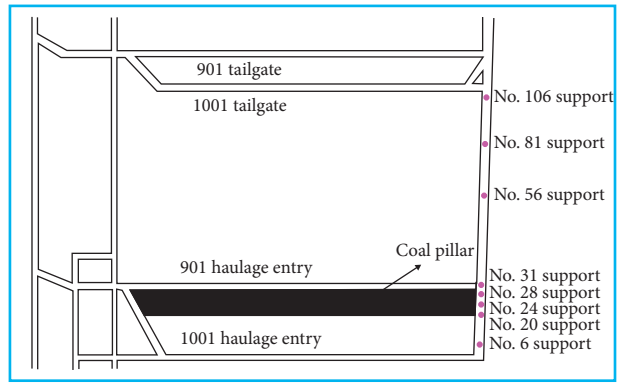

Figure 14: Layout of stations.

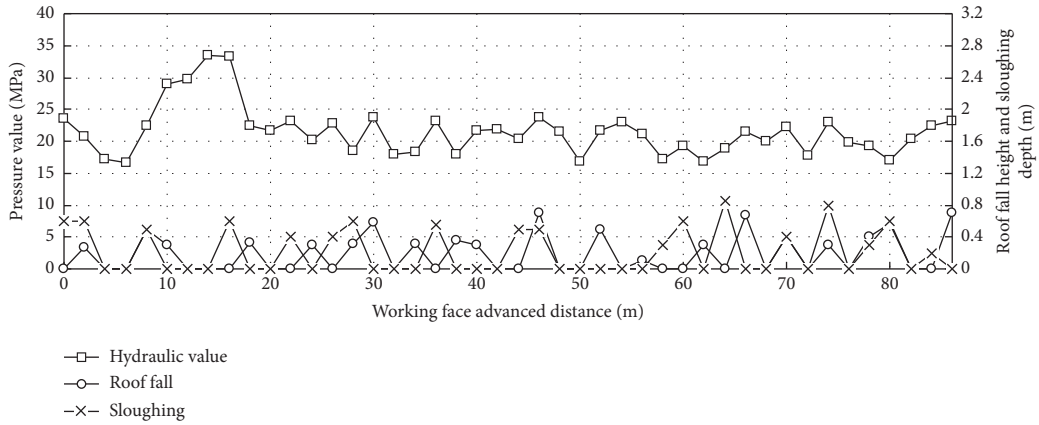

(a)

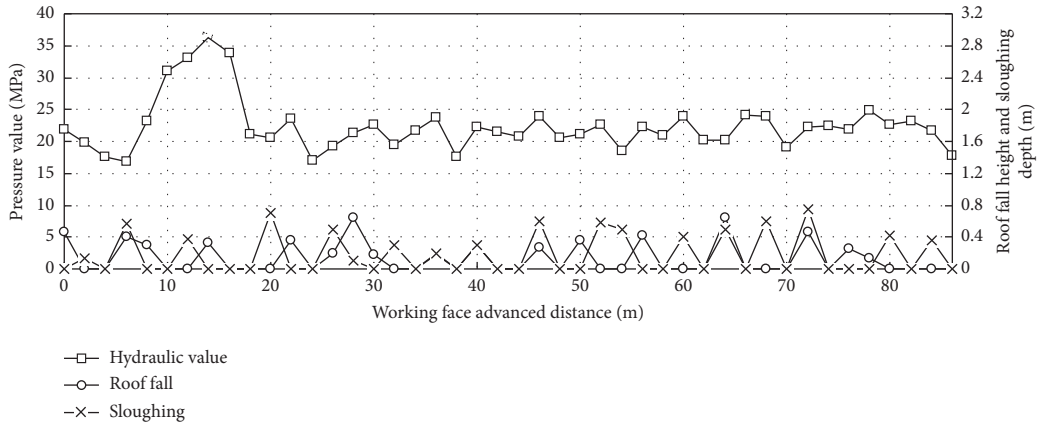

(b)

Figure 15: Continued.

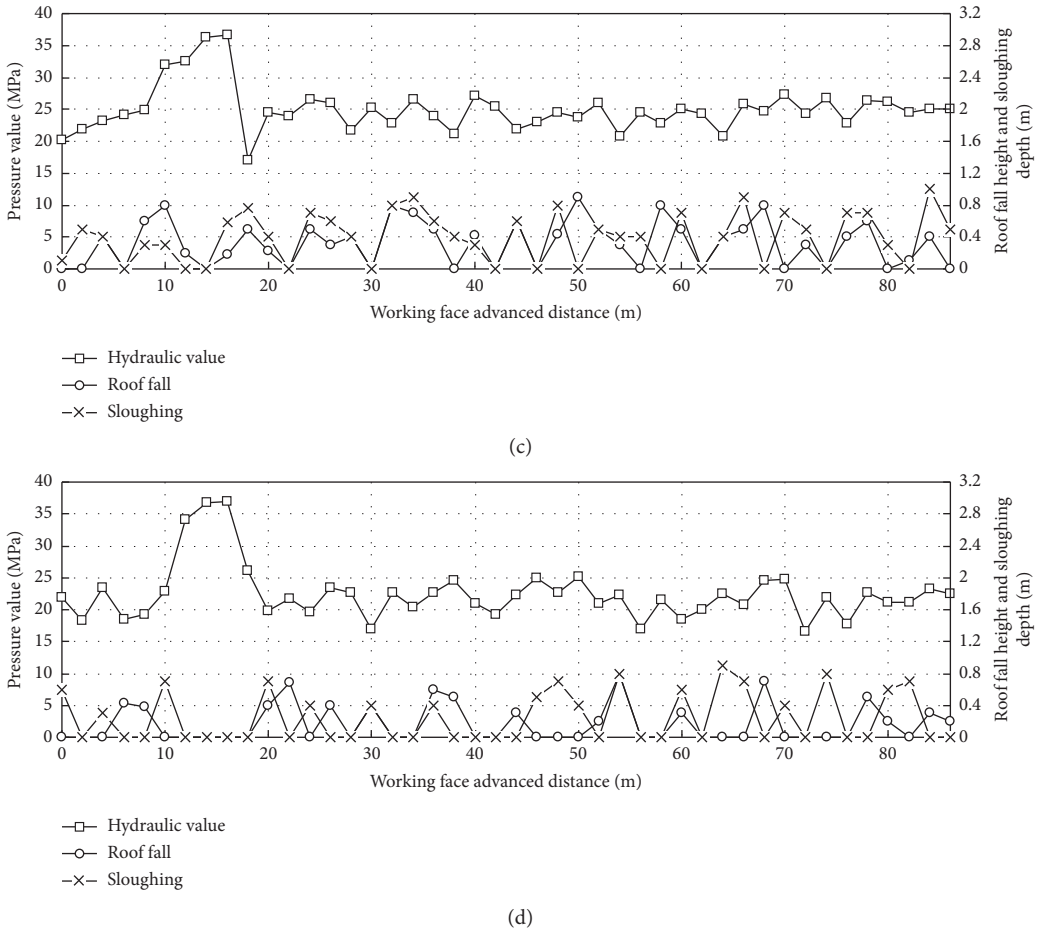

Figure 15: Hydraulic information of support and variation characteristics of roof fall and sloughing. (a) Upper region; (b) middle region; (c) coal pillar region; (d) lower region.

Eight stations were arranged in the working face. The stations were densely distributed under the coal pillar and evenly distributed in other places, as shown in Figure 14. The stations were located at hydraulic support nos. 6, 20, 24, 28, 31, 56, 81, and 106.

6.2. Analysis of Observation Results. The collected hydraulic information of all supports was divided into four regions: the upper, middle, coal pillar, and lower regions. The pressure values of the hydraulic support and the change characteristics of the roof fall and sloughing in each region were considered, as shown in Figure 15.

From the data, it can be concluded that the first collapse steps of the immediate roof in the upper, middle, coal pillar, and lower regions of the working face are 16, 16, 14.5, and 14.3 m, respectively. Comprehensive analysis shows that the average first collapse step of the immediate roof in 1001 working face is 15 m and no obvious periodic weighting is shown, which is consistent with the physical similarity simulation results. The hydraulic value of the support, roof fall height, and sloughing depth in the entire working face reached the maximum at the coal pillar, and the extreme points at the coal pillar were relatively concentrated. Furthermore, maximum points appeared at the upper and lower regions, but the entire working face was not as large as the coal pillar. The hydraulic value of the working face was generally large, roof fall and sloughing occurred occasionally, and preventive measures must be improved.

7. Conclusions

In this study, the physical similitude modeling method was used to study the breakage and migration law of overlying strata in the downward mining of extremely close coal seams, which was verified by field observations in the working face. The conclusions are as follows:

(1) In the process of mining upper coal seam, the first weighting step of the main roof was 37.5 m, and the periodic weighting step was 12.5 m. The occurrence of strata separation was beneficial to the prediction of roof weighting.

(2) When the working face advanced to 25 m, the rock stratum approximating a parallelogram of height 5 m did not collapse, and the working face was relatively dangerous.

(3) When mining the lower coal seam, the overall pressure of the working face was large, but the periodic weighting of the working face was not obvious. The first collapse step of the immediate roof was 15 m.

(4) When mining the upper and lower coal seams, the subsidence of the monitoring point increased significantly at 17.5 and 15 m, respectively. The roof collapse of the lower coal seam was 2.5 m ahead of that of the upper coal seam.

(5) The hydraulic value of the support, roof fall height, and sloughing depth in the entire working face reached the maximum at the coal pillar, and the extreme points at the coal pillar were relatively concentrated. The hydraulic value of the working face was generally large, roof fall and sloughing occurred occasionally, and preventive measures must be improved.

Data Availability

The data used to support the findings of this research are included within the paper.

Conflicts of Interest

The authors declare that they have no conflicts of interest.

Acknowledgments

This work was supported by the National Natural Science Foundation of China (No. 51974317), the Yue Qi Distinguished Scholar Project (800015Z1138), China University of Mining and Technology, Beijing, and the Fundamental Research Funds for the Central Universities (800015J6).

References

[1] Y. Zhang, G. Feng, M. Zhang et al., "Residual coal exploitation and its impact on sustainable development of the coal industry in China," *Energy Policy*, vol. 96, pp. 534–541, 2016.

[2] X. F. Bai, H. Ding, J. J. Lian et al., "Coal production in China: past, present, and future projections," *International Geology Review*, vol. 60, no. 5-6, pp. 535–547, 2018.

[3] Z. Xie, N. Zhang, D. Qian, C. Han, Y. An, and Y. Wang, "Rapid excavation and stability control of deep roadways for an underground coal mine with high production in Inner Mongolia," *Sustainability*, vol. 10, no. 4, pp. 1160–1176, 2018.

[4] A. J. Das, P. K. Mandal, R. Bhattacharjee, S. Tiwari, A. Kushwaha, and L. B. Roy, "Evaluation of stability of underground workings for exploitation of an inclined coal seam by the ubiquitous joint model," *International Journal of Rock Mechanics and Mining Sciences*, vol. 93, pp. 101–114, 2017.

[5] Y. L. Tan, T. B. Zhao, and Y. X. Xiao, "In situ investigations of failure zone of floor strata in mining close distance coal seams," *International Journal of Rock Mechanics and Mining Sciences*, vol. 47, no. 5, pp. 865–870, 2010.

[6] Y. Yuan, Z. Shen, Q.-F. Wang, and S. Pei, "Long distance wireless sensor networks applied in coal mine," *Procedia Earth and Planetary Science*, vol. 1, no. 1, pp. 1461–1467, 2009.

[7] W. Sui, Y. Hang, L. Ma et al., "Interactions of overburden failure zones due to multiple-seam mining using longwall caving," *Bulletin of Engineering Geology and the Environment*, vol. 74, no. 3, pp. 1019–1035, 2014.

[8] H. Z. Zhu, P. Liu, and Z. Y. Tong, "Numerical simulation research and application on protected layer pressure relief affection under different coal pillar width," *Procedia Engineering*, vol. 84, pp. 818–825, 2014.

[9] B. A. Poulsen, "Coal pillar load calculation by pressure arch theory and near field extraction ratio," *International Journal of Rock Mechanics and Mining Sciences*, vol. 47, no. 7, pp. 1158–1165, 2010.

[10] S. R. Xie, Y. J. Sun, S. S. He, E. P. Li, S. Gong, and S. J. Li, "Distinguishing and controlling the key block structure of close-spaced coal seams in China," *Journal of the Southern African Institute of Mining and Metallurgy*, vol. 116, no. 7, pp. 1119–1126, 2016.

[11] W. Y. Guo, Q. H. Gu, Y. L. Tan, and S. C. Hu, "Case studies of rock bursts in tectonic areas with facies change," *Energies*, vol. 12, no. 7, pp. 1–11, 2019.

[12] T. Liu, B. Q. Lin, W. Yang, T. Liu, and C. Zhai, "An integrated technology for gas control and green mining in deep mines based on ultra-thin seam mining," *Environmental Earth Sciences*, vol. 76, no. 6, pp. 243–259, 2017.

[13] W. Y. Guo, Y. L. Tan, F. H. Yu et al., "Mechanical behavior of rock-coal-rock specimens with different coal thicknesses," *Geomechanics and Engineering*, vol. 15, no. 4, pp. 1017–1027, 2018.

[14] G. Cheng, C. Chen, L. Li et al., "Numerical modelling of strata movement at footwall induced by underground mining," *International Journal of Rock Mechanics and Mining Sciences*, vol. 108, pp. 142–156, 2018.

[15] Y. L. Huang, J. X. Zhang, B. F. An, and Q. Zhang, "Overlying strata movement law in fully mechanized coal mining and backfilling longwall face by similar physical simulation," *Journal of Mining Science*, vol. 47, no. 5, pp. 618–627, 2011.

[16] Z. Yuan, Y. Shao, and Z. Zhu, "Similar material simulation study on protection effect of steeply inclined upper protective layer mining with varying interlayer distances," *Advances in Civil Engineering*, vol. 2019, Article ID 9849635, 14 pages, 2019.

[17] Y. Niu, Z. Li, B. Kong et al., "Similar simulation study on the characteristics of the electric potential response to coal mining," *Journal of Geophysics and Engineering*, vol. 15, no. 1, pp. 42–50, 2018.

[18] M. Zhang, Y. Zhang, M. Ji, H. Guo, and H. Li, "Research on physical similarity simulation of mining uphill and downhill at the large-angle working face," *Advances in Civil Engineering*, vol. 2019, Article ID 7696752, 19 pages, 2019.

[19] G. Wu, X. Q. Fang, H. L. Bai, M. F. Liang, and X. K. Hu, "Optimization of roadway layout in ultra-close coal seams: a case study," *PLoS One*, vol. 13, no. 11, Article ID e0207447, 2018.

[20] J. Ning, J. Wang, Y. Tan, L. Zhang, and T. Bu, "In situ investigations into mining-induced overburden failures in close multiple-seam longwall mining: a case study," *Geomechanics and Engineering*, vol. 12, no. 4, pp. 657–673, 2017.

[21] G.-c. Zhang, F.-l. He, H.-g. Jia, and Y.-h. Lai, "Analysis of gateroad stability in relation to yield pillar size: a case study," *Rock Mechanics and Rock Engineering*, vol. 50, no. 5, pp. 1263–1278, 2017.

[22] H. Yan, M. Y. Weng, R. M. Feng, and W. K. Li, "Layout and support design of a coal roadway in ultra-close multiple-

seams," *Journal of Central South University*, vol. 22, no. 11, pp. 4385–4395, 2015.

[23] H. H. Yuan, R. L. Shan, and X. G. Su, "Deformation characteristics and stability control of a gateroad in fully mechanized mining with large mining height," *Arabian Journal of Geosciences*, vol. 11, no. 24, pp. 1–15, 2018.

[24] D. Zhang, W. Sui, and J. Liu, "Overburden failure associated with mining coal seams in close proximity in ascending and descending sequences under a large water body," *Mine Water and the Environment*, vol. 37, no. 2, pp. 322–335, 2018.

[25] P. Zhang, B. Tulu, M. Sears, and J. Trackemas, "Geotechnical considerations for concurrent pillar recovery in close-distance multiple seams," *International Journal of Mining Science and Technology*, vol. 28, no. 1, pp. 21–27, 2018.

[26] Y. Yu, K.-Z. Deng, and S.-E. Chen, "Mine size effects on coal pillar stress and their application for partial extraction," *Sustainability*, vol. 10, no. 3, pp. 792–803, 2018.

[27] W.-b. Zhu, J.-l. Xu, X. Kong, D.-y. Xuan, and W. Qin, "Study on pillar stability of Wongawilli mining area in shallow close distance coal seams," *Procedia Earth and Planetary Science*, vol. 1, no. 1, pp. 235–242, 2009.

[28] W. Zhang, D. Zhang, D. Qi, W. Hu, Z. He, and W. Zhang, "Floor failure depth of upper coal seam during close coal seams mining and its novel detection method," *Energy Exploration & Exploitation*, vol. 36, no. 5, pp. 1265–1278, 2018.

[29] X. J. Liu, X. M. Li, and W. D. Pan, "Analysis on the floor stress distribution and roadway position in the close distance coal seams," *Arabian Journal of Geosciences*, vol. 9, no. 2, pp. 83–90, 2016.

[30] X. H. Li, S. Liang, Q. L. Yao, and Q. D. Qu, "Disaster-causing mechanism of gateroad under ultra-close gob of board-pillar mining working face and its control," *Disaster Advances*, vol. 6, pp. 244–259, 2013.

[31] B. Ghabraie, K. Ghabraie, G. Ren, and J. V. Smith, "Numerical modelling of multistage caving processes: insights from multi-seam longwall mining-induced subsidence," *International Journal for Numerical and Analytical Methods in Geomechanics*, vol. 41, no. 7, pp. 959–975, 2017.

[32] M. Khanal, D. Adhikary, C. Jayasundara, and R. Balusu, "Numerical study of mine site specific multiseam mining and its impact on surface subsidence and chain pillar stress," *Geotechnical and Geological Engineering*, vol. 34, no. 1, pp. 217–235, 2016.

[33] H. Wang, Y. Cheng, and L. Yuan, "Gas outburst disasters and the mining technology of key protective seam in coal seam group in the Huainan coalfield," *Natural Hazards*, vol. 67, no. 2, pp. 763–782, 2013.

[34] P. Konicek and Schreiber, "Rockburst prevention via destress blasting of competent roof rocks in hard coal longwall mining," *Journal of the Southern African Institute of Mining and Metallurgy*, vol. 118, no. 3, pp. 235–242, 2018.

[35] J. Zhang, J. Peng, W. Liu, and W. Lu, "Predicting resilient modulus of fine-grained subgrade soils considering relative compaction and matric suction," *Road Materials and Pavement Design*, vol. 1, pp. 1–13, 2019.

[36] S. Ren, D. Y. Jiang, C. H. Yang, and J. Chen, *Mining Subsidence and Cavity Stability during Halite Dissolve Mining*, Chongqing University Press, Chongqing, China, 2012.

[37] Q. S. Wu, L. S. Jiang, Q. L. Wu, Y. C. Xue, and B. Gong, "A study on the law of overlying strata migration and separation space evolution under hard and thick strata in underground coal mining by similar simulation," *Dyna*, vol. 93, no. 2, pp. 175–181, 2018.